Thermodynamic Analysis and Optimization of RWGS Processes for Solar Syngas Production from CO_2

Marcus Wenzel[1], Liisa Rihko-Struckmann[1], and Kai Sundmacher[1,2]

[1]Max-Planck-Institute for Dynamics of Complex Technical Systems, Sandtorstr. 1, 39106 Magdeburg, Germany

[2]Otto-von-Guericke-University Magdeburg, Universitätsplatz 2, 39106 Magdeburg, Germany

Abstract

Process systems were investigated for syngas production from CO_2 and renewable energy (solar) by the reverse water-gas shift (RWGS) and the reverse water-gas shift chemical looping (RWGS-CL) process. Thermodynamic analysis and optimization was performed to maximize the solar-to-syngas (StS) efficiency η_{StS}. Special emphasis was laid on product gas separation. For RWGS-CL, a maximum StS efficiencies of 14.2 and 14.4% were achieved without and with heat integration, respectively. The StS efficiency is dictated by the low overall efficiency of H_2 production. RWGS-CL is most beneficial for the production of pure CO, where the StS efficiency is one percent point higher compared to that of the RWGS process with heat integration. Heat integration leads to significant reductions in external heat demand since most of the gas phase process heat can be integrated. The StS efficiencies for RWGS and RWGS-CL achieve the same level as the reported values for solar thermochemical syngas production.

Introduction

Mitigating the exhaust of CO_2 into the atmosphere from burning fossil fuels is critical for reducing the negative effects on the world's climate[1]. To overcome the dependency on fossil fuels, an alternative carbon source (e.g. CO_2) and efficient and sustainable technologies for the production of bulk

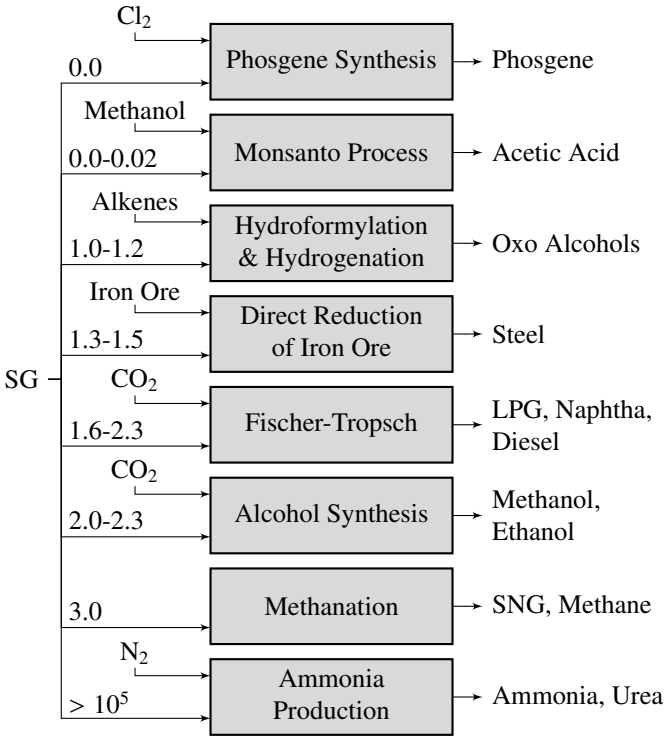

Figure 1: Most important syngas (SG) applications. Numbers indicate the H_2/CO ratio required by the respective process.

chemicals are needed. Syngas is a central precursor for the sythesis of a wide range of products (Figure 1). Typically, syngas is produced from fossil sources, most notably natural gas, naphtha and coal[2]. However, syngas can be produced by CO_2 and renewable energy sources by using the reverse water-gas shift (RWGS) reaction. Mallapragada *et al.* estimated higher current and future sun-to-fuel efficiency for the conversion of CO_2 *via* the RWGS reaction as a key step compared to other emerging technologies[3]. An intensified version of the conventional RWGS reaction is RWGS chemical looping (RWGS-CL), in which the RWGS reaction is split into two stages by applying an oxygen carrier material (often a metal oxide)[4–6]. The most important advantage of this approach is the inherent partial gas separation, which potentially reduces the energy demand for product gas treatment. Furthermore, Romero and Steinfeld stated that solar syngas production from H_2O and CO_2 *via* two-step redox cycles has favorable long-term potential[7].

However, energy efficiency is a crucial factor in CO_2 utilization processes, since they are naturally energy intensive. One method to assess the energy efficiency for a given process is the analysis based on the first and second law of thermodynamics. While thermodynamic analysis has been applied extensively to solar thermochemical syngas production processes[8–13], a systematic comparison of RWGS and RWGS-CL has not yet been conducted. Furthermore, the direct comparison of reported

energy efficiencies for solar thermochemical syngas production is difficult because each research group defines the system boundaries differently. An analysis with comparable system boundaries will enable us to identify the most promising concepts for energy efficient CO_2 conversion to syngas.

In this work, process systems are designed for the conventional RWGS and the RWGS-CL process for syngas production from CO_2 and renewable energy (solar). The systems are optimized in terms of energy efficiency and the results are compared and discussed. Special emphasis is put on the gas separation after reaction. Marxer *et al.* reported that syngas with 30.5% unreacted CO_2 was obtained for the solar thermochemical ceria cycle[14]. While some downstream operations (e.g. Fischer-Tropsch) are not affected by remaining CO_2, other applications require the removal of CO_2 and/or H_2O from syngas. Even though it has been shown that the separation of reactants from the products affects the overall process efficiency[15,16], gas separation is ignored in the efficiency calculation in many studies. Here, we use literature data of separation processes to include gas separation in the analysis. The aim is to predict realistic efficiencies for sustainable syngas production systems using CO_2.

Process Systems

Reverse Water-Gas Shift (RWGS)

A flow sheet of the conventional reverse water-gas shift (RWGS) process for CO_2 conversion to syngas is depicted in Figure 2. Solar energy is used to produce heat and power for the process. Water (1) is electrolyzed to produce H_2 (2a), which reacts with CO_2 (3) in the RWGS unit to form a mixture of syngas, water and CO_2 (4), according to the following reaction:

$$\text{RWGS:} \qquad H_2 + CO_2 \rightleftharpoons H_2O + CO \qquad \Delta H_R(1073\,\text{K}) = 36.84\text{kJ/mol} \qquad (1)$$

The majority of water can be removed by condensation in a flash unit (5b). The remaining gas (5a) is separated in a separation unit to yield pure component streams. Residual water after the flash unit is assumed to be removed in the gas phase (6d). Unreacted CO_2 is recycled to the RWGS unit (6b). To obtain syngas with a low H_2/CO ratio, H_2 might be recycled to the reactor (6c). In the conventional RWGS process, the H_2/CO ratio of the product syngas (8) can be adjusted either by varying the feed H_2/CO_2 ratio or by keeping the initial H_2/CO_2 ratio constant and adding additional H_2 after the reaction (7). By definition, the arrow of the heat streams always points toward the

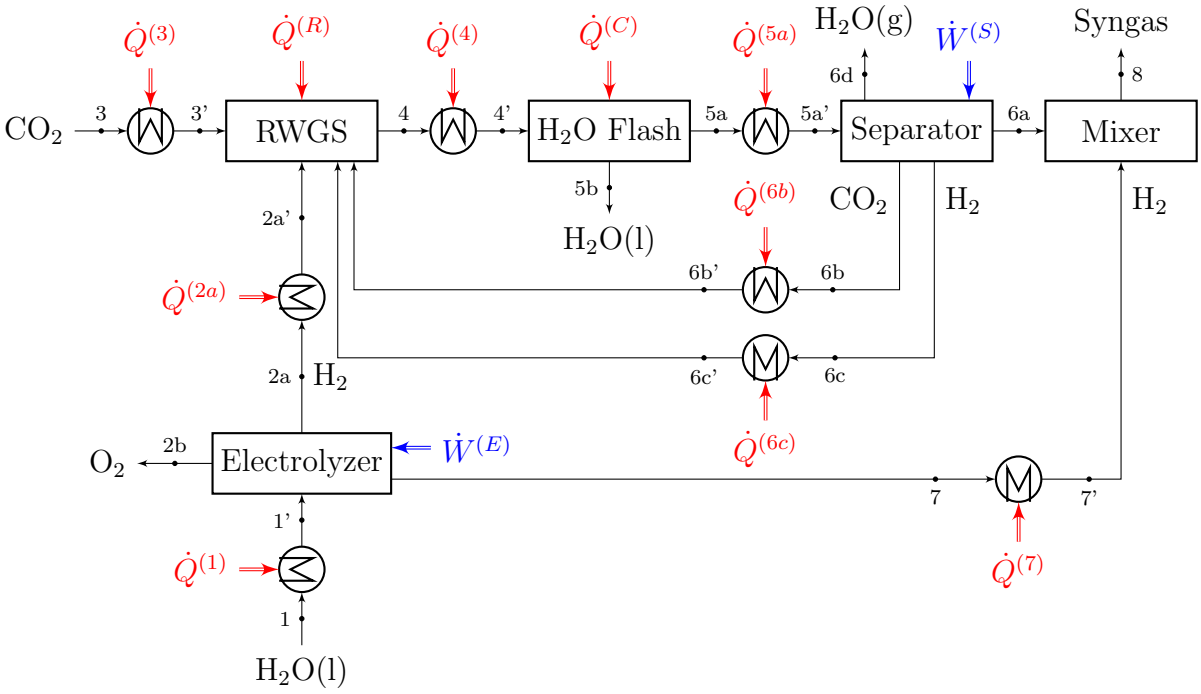

Figure 2: Idealized process system for syngas production by RWGS.

units. This, however, does not imply the actual direction of heat transfer (heat flow out of a unit is signed negative).

Reverse Water-Gas Shift Chemical Looping (RWGS-CL)

Figure 3 shows a flow sheet for the RWGS-CL process. While there are several similarities to the conventional RWGS process, some crucial differences do exist. Note, however, that the system boundaries remain unchanged allowing fair process comparison. In the electrolyzer, H_2 (2a) is produced by electrolysis. Since the RWGS-CL unit is a two-stage process with spatially separated reactions, CO_2 and H_2 enter the reactor at separate locations (CO_2 for oxidation and H_2 for reduction of the material). For the RWGS-CL reactor, the reaction equations can be expressed as

$$\text{Oxidation:} \qquad 3/4\,\text{Fe} + \text{CO}_2 \rightleftharpoons 3/4\,\text{FeO}_{4/3} + \text{CO} \qquad \Delta H_R(1073K) = 8.98\,\text{kJ/mol} \tag{2}$$

$$\text{Reduction:} \qquad 3/4\,\text{FeO}_{4/3} + \text{H}_2 \rightleftharpoons 3/4\,\text{Fe} + \text{H}_2\text{O} \qquad \Delta H_R(1073K) = 27.86\,\text{kJ/mol} \tag{3}$$

The most simple RWGS-CL reactor consists of at least two fixed bed reactors: one for the reduction and one for the oxidation reaction. Upon complete conversion of solid iron (oxide) the gas flows to the reactors are switched, ideally allowing a quasi-continuous operation. More complex reactor designs are currently investigated to enhance reaction kinetics and heat transfer[17,18]. The oxidation

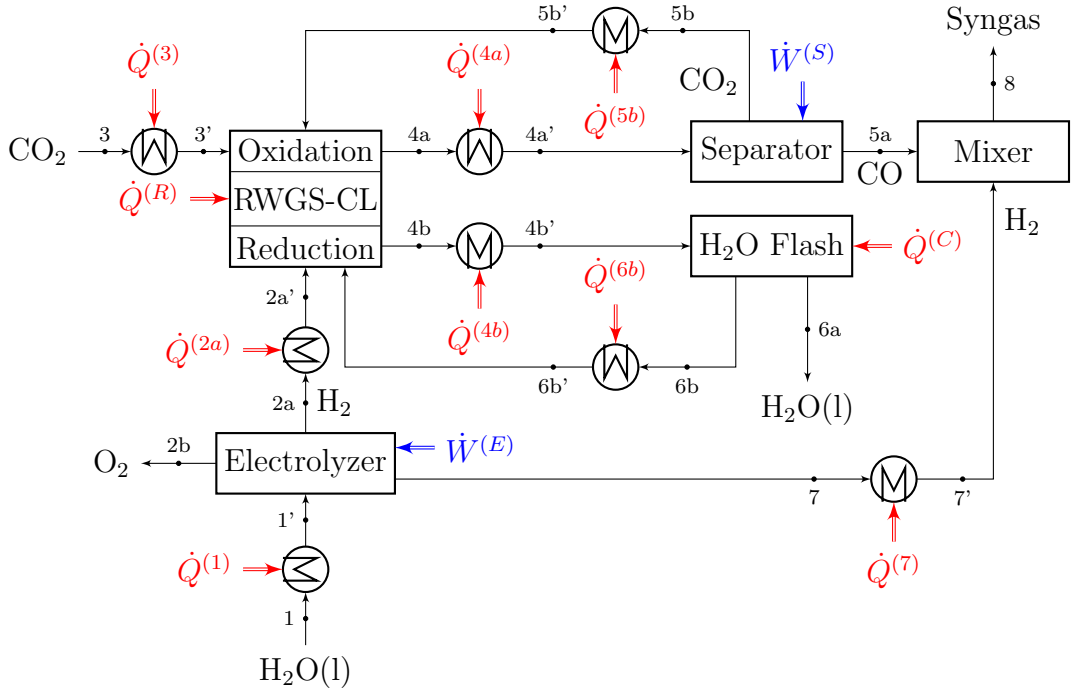

Figure 3: Idealized process system for syngas production by RWGS-CL.

reactor outlet (4a) contains a mixture of CO_2 and CO, which must be separated. The unreacted CO_2 is fed back to the oxidation stage of reactor (5b). The reduction reactor outlet (4b) contains H_2O, which is separated by condensation (6a), and H_2, which is recycled to the reduction stage of the reactor (6b). Due to phase equilibrium in the flash unit, the hydrogen stream (6b) is saturated with water vapor. The H_2/CO ratio of the syngas is adjusted by adding H_2 (7) to the CO stream (5a) to yield the desired product syngas (8). It is also conceivable to use some fraction of stream (6b) to adjust the H_2/CO ratio in the mixer. However, H_2 from stream (7) is always preferable because it bypasses heating and cooling in the reactor/separator sequence and, thus, contributes less to the total energy demand.

Thermodynamic Model

Modeling of an ideal process systems entails a number of assumptions. All gases are treated as ideal gases. Potential and kinetic energies are neglected. The gas composition in the heaters and coolers remains unchanged (no chemical reactions occur). The systems operate at atmospheric pressure. Specific assumptions for each operation are discussed in the following sections.

Solar Energy Collection

It is assumed that high temperature heat from solar energy is readily available, which supplies the necessary heat for the process units. Solar energy ($\dot{Q}^{(solar)}$) is assumed to be absorbed by a black body receiver. Losses in solar collection and thermal losses due to reradiation ($\dot{Q}^{(rerad)}$) are accounted for by the solar energy collection (SEC) efficiency, which is defined as

$$\eta_{SEC} = \frac{L_H(\dot{Q}^{(solar)} - \dot{Q}^{(rerad)})}{\dot{Q}^{(solar)}} = \frac{L_H\left(G_0 C - \sigma(T^{(R)})^4\right)}{G_0 C}. \tag{4}$$

Here, L_H in an adjustable parameter for the total heat loss of the system and $\dot{Q}^{(rerad)}$ accounts for losses due to reradiation. Heat loss factors of $L_H = 0.8$[10] and 0.9[9] were used in studies for solar thermochemical processes at temperatures above 1273 K. The heat losses are assumed to be lower in this analysis since the highest temperature in the reactor is 1073 K. Thus, a heat loss factor of $L_H = 0.95$ is assumed. G_0 is the nominal solar flux incident on the concentrator. Its value is assumed to be $1\,\mathrm{kW/m^2}$[10] which is slightly lower than the mean solar irradiance on earth ($1.37\,\mathrm{kW/m^2}$[19]). The solar concentration factor C is set to 3000 suns, which can be achieved by Dish-Sterling concentrators[20]. Reradiation losses depend on the temperature of the RWGS reactor ($T^{(R)}$)[10]. It should be noted, however, that this approximation assumes that all solar heat to the system is supplied at reactor temperature (1073 K) even though some of the process heat is required at a lower temperature. This leads to a slight overestimation of reradiation losses.

Electrolysis

Water for electrolysis is supplied at ambient temperature ($T^{(0)} = 298\,\mathrm{K}$) and electrolysis is performed at 353 K which is typical for alkaline or PEM electrolyzers[21,22]. Their specific electrical energy demand is approximately $5.5\,\mathrm{kWh/Nm^3_{H_2}}$ or $444\,\mathrm{kJ/mol_{H_2}}$[22]. This includes purification of the produced hydrogen up to 99.8%[23]. Therefore, the produced hydrogen can be considered practically pure for the efficiency analysis. The energy for electrolysis is assumed to be generated from solar energy by a Dish-Sterling power system with a solar-to-electricity (StE) efficiency of $\eta_{StE} = 0.25$[20]. Thus, the corresponding solar heat required for the electrolyzer ($\dot{Q}^{(E)}$) is given by

$$\dot{Q}^{(E)} = \frac{\dot{W}^{(E)}}{\eta_{StE}} = \frac{444\,\mathrm{kJ/mol_{H_2}}(\dot{N}^{(2a)}_{H_2} + \dot{N}^{(7)}_{H_2})}{\eta_{StE}}. \tag{5}$$

Reactor

Concentrated CO_2 is assumed to be available at 313 K, which is preheated to the reactor temperature $T^{(R)}$ prior to entering the reactor. It is assumed that chemical equilibrium is achieved in the reactor for RWGS and RWGS-CL. The heat that must be supplied to the RWGS reactor is calculated by

$$\dot{Q}^{(RWGS)} = \Delta H_R^{(RWGS)} \dot{\xi}^{(RWGS)}, \tag{6}$$

where $\dot{\xi}^{(RWGS)}$ is the reaction extent per unit time of the RWGS reaction. For RWGS-CL, the heat of reaction for oxidation and reduction can be calculated analogously:

$$\dot{Q}^{(RWGS-CL,O)} = \Delta H_R^{(RWGS-CL,O)} \dot{\xi}^{(RWGS-CL,O)} \tag{7}$$

$$\dot{Q}^{(RWGS-CL,R)} = \Delta H_R^{(RWGS-CL,R)} \dot{\xi}^{(RWGS-CL,R)} \tag{8}$$

The overall heat demand of the RWGS-CL reactor includes the heat required for the oxidation and reduction reaction:

$$\dot{Q}^{(RWGS-CL)} = \dot{Q}^{(RWGS-CL,O)} + \dot{Q}^{(RWGS-CL,R)} \tag{9}$$

For both RWGS and RWGS-CL, the reactor temperature is set to 1073 K, which is typical for iron oxide. This temperature ensures adequate rates of reaction while minimizing temperature related problems (e.g. material sintering). In RWGS-CL, both reactors operate at 1073 K. The RWGS reaction and RWGS-CL reactions are mildly endothermic and the heat of reaction depends weakly on the temperature. The equilibrium constants (K_{eq}) for the RWGS reaction and the RWGS-CL reactions are depicted in Figure 4 as a function of temperature. For $T > 1093$ K, the reaction equilibrium for the RWGS reaction (eq. (1)) lies on the product side ($K_{eq} > 1$). For the oxidation reaction of RWGS-CL (eq. (2)) this is the case for the whole range of temperature inspected, while the equilibrium of the reduction reaction (eq. (3)) lies on the product side only at temperatures above 1273 K. The higher K_{eq} of the oxidation reaction in RWGS-CL results in a higher equilibrium CO_2 conversion and lower CO_2 content in the CO/CO_2 mixture compared to the conventional RWGS reaction. This comes at the cost of decreased conversion of H_2 in the reduction reaction. However, since a H_2/H_2O mixture is easier to separate (e.g. by condensation) than a CO/CO_2 mixture, this gives a potential advantage of RWGS-CL over RWGS, most notably for the production of pure CO.

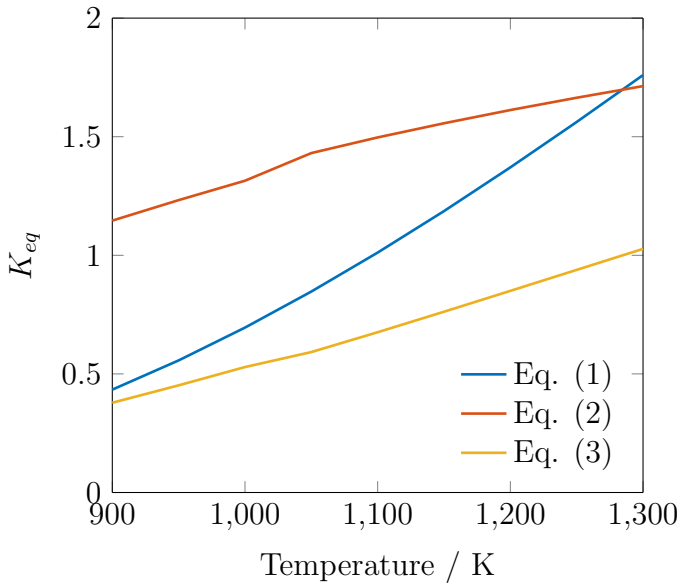

Figure 4: Temperature dependence of the equilibrium constant K_{eq} for the RWGS reaction (Eq. (1)) and for the RWGS-CL reactions with iron oxide (Eq. (2) and (3)).

H_2O Flash

Water is separated from the product gas by condensation at 313 K. The gas and liquid outlet streams are assumed to be in phase equilibrium. For the RWGS process, the energy released during condensation can be calculated from the enthalpy balance according to

$$\dot{Q}^{(C)} = -\dot{H}^{(4')} + \dot{H}^{(5a)} + \dot{H}^{(5b)}, \tag{10}$$

where $\dot{H}$ is the enthalpy flow which can be calculated from the molar flow $\dot{N}$ and the molar enthalpy $h(T)$ by

$$\dot{H} = \dot{N}h(T). \tag{11}$$

For the RWGS-CL process, an analogous relationship is used (see Figure 3).

Separator

For an ideal separation unit with one inlet stream and N_{out} outlet streams, the minimum thermodynamic energy of separation (=reversible energy) under isothermal and isobaric conditions is given

by

$$\dot{W}_{rev}^{(S)} = -RT \left(\sum_{\alpha}^{N_C} \dot{N}_\alpha \ln x_\alpha - \sum_{i}^{N_{out}} \sum_{\alpha}^{N_C} \dot{N}_\alpha^{(i)} \ln x_\alpha^{(i)} \right), \tag{12}$$

where N_C is the number of components in each stream. However, the reversible work $\dot{W}_{rev}^{(S)}$ is a poor estimate of the actual work needed to separate gases[24,25], which depends strongly on the specific separation technology that is used (e.g. absorption, adsorption or distillation). The ratio of the reversible energy of separation to the actual energy can be expressed by the separation efficiency, defined as

$$\eta_S = \frac{\dot{W}_{rev}^{(S)}}{\dot{W}_{act}^{(S)}}. \tag{13}$$

The separation efficiency for real separation processes lies in the range of $5 - 40\%$[26]. House *et al.*[26] and Wilcox[24] reviewed the separation efficiencies for typical separation processes in industry. Based on this information, we estimate the separation efficiency as a function of the initial mole fraction of the component that is separated. While the data points for the separation efficiency span a wide range, the trend is that a low initial mole fraction leads to a low separation efficiency. In Figure 5, the data points are shown together with the least squares fit of a nonlinear model $\eta_S = f(x_\alpha)$. The correlation $\eta_S = f(x_\alpha)$ is used to estimate the actual energy from the reversible energy of a separation process. The actual energy of separation is assumed to be generated by solar energy with a StE efficiency of $\eta_{StE} = 0.25$[20]. Thus, the actual energy demand for separation can be expressed in terms of the solar heat required by

$$\dot{Q}^{(S)} = \frac{\dot{W}_{rev}^{(S)}}{\eta_S \eta_{StE}}. \tag{14}$$

The gases are assumed to be separated at a temperature of 313 K, which is typical for a monoethanolamine (MEA) absorption process for CO_2 separation[24].

Heating and Cooling

Heating and/or cooling of the process streams is necessary since each unit operates at a specific temperature. The energy for heating is supplied by solar energy. The streams and the flash unit

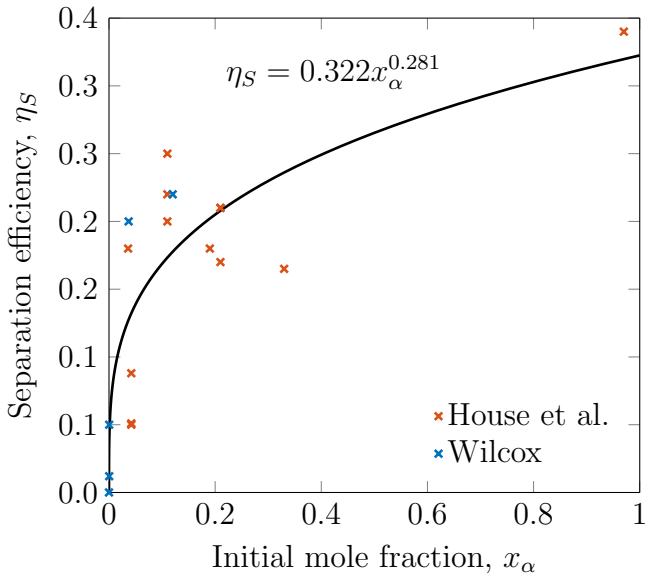

Figure 5: Separation efficiency η_S as a function of the initial mole fraction of the component to be separated. Literature data for real separation process from House *et al.*[26] and Wilcox[24].

($\dot{Q}^{(C)}$) are cooled by water at ambient temperature. Since all process streams have temperatures $\geq 313\,\mathrm{K}$, water at 298 K can be used for cooling and expensive refrigeration systems are not necessary. Assuming that the energy demand for pumping the water is negligible, cooling of the process streams does not affect the StS efficiency. The overall amount of energy required for stream heating is summarized by $\dot{Q}^{(Stream)}$, which is calculated by

$$\dot{Q}^{(Stream)} = \sum_{k}^{N_S} \dot{Q}^{(k)}, \tag{15}$$

where k is the identifier of the heater and N_S is the total number of streams to be heated. For RWGS, $k = \{1, 2\mathrm{a}, 3, 6\mathrm{b}, 6\mathrm{c}\}$ (see Figure 2) and for RWGS-CL, $k = \{1, 2\mathrm{a}, 3, 5\mathrm{b}, 6\mathrm{b}\}$ (see Figure 3). The heat demand for heater k can be calculated by

$$\dot{Q}^{(k)} = \dot{N}^{(k)} \int_{T^{(k)}}^{T^{(k')}} c_p^{(k)}(T)\mathrm{d}T, \tag{16}$$

where $c_p^{(k)}(T)$ is the temperature dependent molar heat capacity of stream k, and $T^{(k)}$ and $T^{(k')}$ are the temperatures before and after the heater/cooler, respectively.

Mixer

No heat is produced during mixing since the enthalpy change of mixing is zero for ideal gases.

Results and Discussion

The idealized process systems are evaluated using the solar-to-syngas (StS) efficiency η_{StS}, which is defined as

$$\eta_{StS} = \frac{\eta_{SEC}\left(\dot{N}_{\mathrm{H_2}}^{(8)}\mathrm{HHV}_{\mathrm{H_2}} + \dot{N}_{\mathrm{CO}}^{(8)}\mathrm{HHV}_{\mathrm{CO}}\right)}{\dot{Q}^{(E)} + \dot{Q}^{(Stream)} + \dot{Q}^{(R)} + \dot{Q}^{(S)}} \tag{17}$$

where HHV is the higher heating value and $\dot{Q}^{(E)}$, $\dot{Q}^{(Stream)}$, $\dot{Q}^{(R)}$ and $\dot{Q}^{(S)}$ are the energy demands for the electrolyzer, stream heating, reactor heating and gas separation, respectively. It is convenient to express these terms as dimensionless energy factors F by normalizing each $\dot{Q}$ by the energy stored chemically (HHV) in the product syngas[27]:

$$\eta_{StS} = \frac{\eta_{SEC}}{F^{(E)} + F^{(Stream)} + F^{(R)} + F^{(S)}} \tag{18}$$

The relative magnitude of each F factor indicates which process contributes most to the total energy demand.

The idealized process systems are optimized to yield the maximum StS efficiency, η_{StS}. The optimization variables are the molar flows $\dot{N}_{\alpha}^{(i)}$ where i denotes streams 1 to 8 and the reaction extent of the electrolyzer ($\dot{\xi}^{(E)}$) and the reactor ($\dot{\xi}^{(R)}$). They constitute a nonlinear programming problem (NLP) which is solved with the *fmincon* function in MATLAB:

$$\begin{aligned} \min_{\dot{N}_{\alpha}^{(i)}, \dot{\xi}^{(E)}, \dot{\xi}^{(R)}} \quad & 1/\eta_{StS} \\ \text{s.t.} \quad & \text{Mass balances} \\ & \text{Eq. (6) to (18)} \\ & 0 \leq \dot{N}_{\alpha}^{(i)} \leq 1\,\mathrm{mol/s} \\ & 0 \leq \dot{\xi}^{(E)} \leq 1\,\mathrm{mol/s} \\ & 0 \leq \dot{\xi}^{(R)} \leq 1\,\mathrm{mol/s} \end{aligned} \tag{19}$$

Pinch analysis was included in the optimization for heat integration of the streams[28]. Thus, the influence of heat integration on the optimal solution could be investigated. For the case with heat integration, $\dot{Q}^{(Stream)}$ includes only the heat that has to be provided by external sources. The

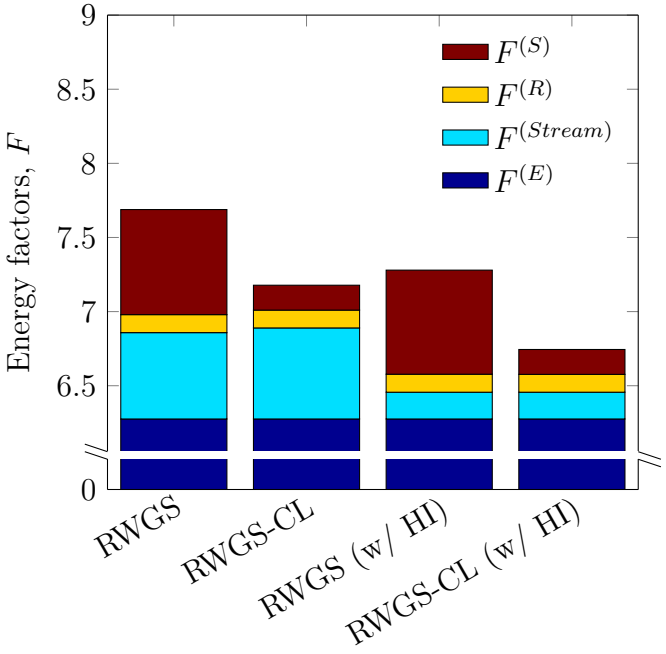

Figure 6: Dimensionless energy factors F for pure CO production. RWGS and RWGS-CL refer to the process schemes in Figures 2 and 3, respectively. Results with heat integration are denoted by (w/ HI).

considered heating and cooling duties for heat integration were all $\dot{Q}$ except for $\dot{Q}^{(R)}$ since reactor heating is considered separately. The minimum temperature difference at the pinch point was set to 10 K. The heat integration network depends on the optimal solution and is, therefore, not depicted in Figure 2 or 3.

Optimization Results

Figure 6 shows the F values for pure CO production by RWGS and RWGS-CL with and without gas phase heat integration. With a value of $F^{(E)} = 6.27$, the electrolyzer is dominating the overall energy demand in all cases contributing to more than 80%. This is mainly due to the low StE efficiency for electricity generation. The second largest contributor to the overall energy demand is stream heating ($F^{(Stream)}$) with approximately 8% for the cases without heat integration. The energy demand for reactor heating ($F^{(R)}$) only accounts for approximately 2% of the total energy demand. Significant reductions in energy consumption can be achieved in the reactor/separator sequence. For the RWGS-CL process, $F^{(S)}$ is reduced by 77% as compared to the RWGS process due to the partial gas separation in the RWGS-CL reactor. Furthermore, heat integration leads to a reduction of $F^{(Stream)}$ by $\approx 70\%$ for both processes. $F^{(Stream)}$ accounts for $\approx 1.5\%$ of the total energy demand

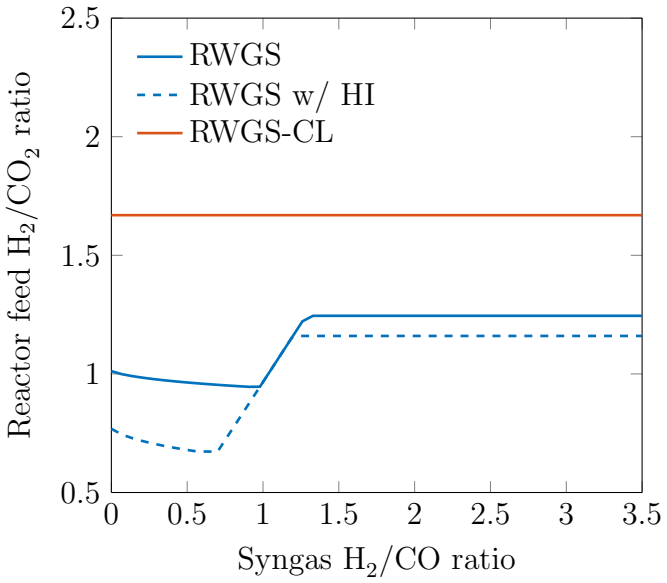

Figure 7: Optimal reactor feed H_2/CO_2 ratios for maximal StS efficiency according to eq. (19). The feed consists of all input streams into the reactor, including recycle streams. RWGS and RWGS-CL correspond to the process schemes 2 and 3, respectively. The line for RWGS-CL with heat integration is identical to the RWGS-CL line.

for the cases with heat integration. A reduction of 54% in the sum of $F^{(Stream)}$, $F^{(R)}$ and $F^{(S)}$ can be achieved by using RWGS-CL compared to RWGS (both cases with heat integration). RWGS-CL without heat integration has a lower overall energy demand than RWGS with heat integration. Thus, RWGS-CL is significantly more efficient in the reactor/separator sequence of the process. This, however, comes at the cost of a more complicated reactor design.

The optimal H_2/CO_2 ratios into the reactor are illustrated in Figure 7. In the RWGS-CL process, the optimal reactor feed ratio is constant for all syngas H_2/CO ratios because the reaction extents for oxidation and reduction are coupled to ensure that the same amount of solid material is oxidized and reduced, which is necessary for quasi-stationary operation. Therefore, a constant value of 1.67 is obtained for the cases with and without gas phase heat integration. For the RWGS process, the optimal H_2/CO_2 ratio in the reactor depends on the desired H_2/CO ratio. In the case without heat integration, the optimal reactor feed ratio declines slightly from 1 to approximately 0.95 for H_2/CO ratios between 0.0 and 1.0. This leads to an increase in the CO_2 mole fraction of the product stream. This is beneficial for the overall efficiency, since the separation efficiency is higher at higher CO_2 concentrations in the separator inlet. The reactor feed ratio increases to approximately 1.25 for H_2/CO ratios > 1. For H_2/CO ratios > 1.4, the reactor feed ratio remains constant and higher H_2/CO ratios are achieved by adding H_2 *via* stream (7) after the reaction, which is beneficial for

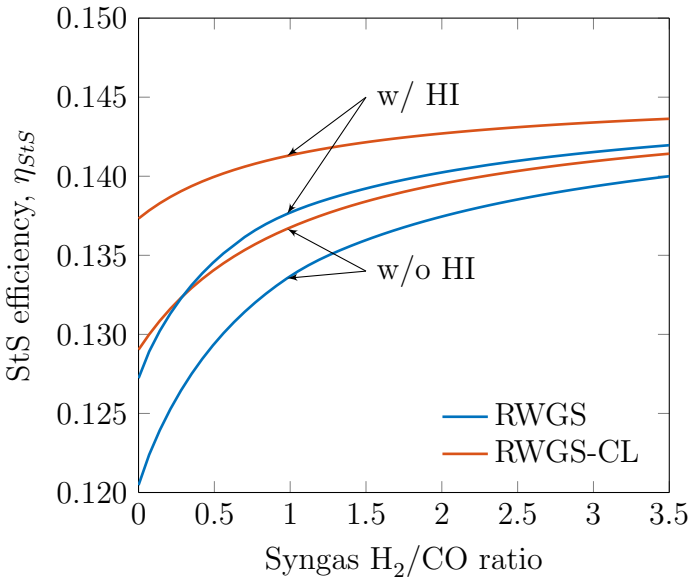

Figure 8: StS efficiency η_{StS} with (w/) and without (w/o) gas phase heat integration (HI) as a function of syngas H_2/CO ratio. Lines for RWGS and RWGS-CL correspond to the process schemes in Figures 2 and 3, respectively.

StS efficiency, as it leads to high degrees of conversions for H_2 and CO_2 in the reactor and therefore minimizes the heat needed for reheating reactants in the recycle. The results indicate that for the RWGS process without heat integration a reactor feed H_2/CO_2 ratio of approximately 1.25 is beneficial for the production of syngas with $H_2/CO > 1.4$. With heat integration enabled, the optimal solution is similar but shifted to lower reactor feed H_2/CO_2 ratios. At these ratios, optimal heat integration is achieved and external heat supply is minimized.

The StS efficiency obtained by optimization with and without gas phase heat integration is shown in Figure 8. With heat integration enabled, the StS efficiency varies between 0.127 and 0.142 for RWGS and between 0.137 and 0.144 for RWGS depending on the desired syngas H_2/CO ratio. With the assumptions made in this analysis, the solar energy collection efficiency is $\eta_{SEC} = 0.926$, i.e. 7.4% of the solar energy input is lost due to reradiation and heat loss in the process. The StS efficiency is increasing with increasing H_2/CO ratios in all cases because the energy demand for gas separation and reheating of reactants decreases as less CO is formed. The maximum StS efficiency for each process is obtained at syngas H_2/CO ratios of 3.5. The StS efficiency at all syngas ratios is dictated by the low overall efficiency of H_2 production. The RWGS-CL process achieves a StS efficiency up to one percent point higher than the RWGS process for all syngas ratios. However, the difference decreases to 0.2 percent points for syngas with $H_2/CO = 3.5$. Thus, the advantage of inherent gas separation in the RWGS-CL reactor is most pronounced for the production of pure CO. Despite the

dominating influence of H_2 production on the energy demand, heat integration leads to efficiencies up to 1 percent point higher compared to the processes without heat integration.

Comparison with Solar Thermochemical Syngas Production

Thermochemical processes for syngas production based on solar heat have been investigated extensively in the last years and are generally considered an important pathway towards CO_2 utilization alongside other emerging technologies[3]. Syngas is produced by simultaneously splitting H_2O and CO_2[17,29]. However, there are several drawbacks to this approach. First, very high temperatures (usually $> 1273\,\mathrm{K}$) and/or reduced pressure are needed for the thermal reduction of the oxygen storage material, resulting in high stability requirements for the reactor and the oxygen storage material[29]. Sintering is a problem that has been addressed extensively in the literature[29,30]. Second, several research groups remarked that solid phase heat recovery between the oxidation and reduction reactions is a critical factor for the overall process efficiency[8–10,31,32]. While new reactor concepts are being developed[18] to address this problem, efficient solid phase heat recovery remains a major issue[29]. Third, the CO yield per solid mass is relatively low for solar thermochemical processes. Reported values in the literature range from $0.15\,\mathrm{mol_{CO}/kg_{CeO_2}}$ for ceria[17] to 0.2-1.0 $\mathrm{mol_{CO}/kg}$ for state-of-the-art perovskite type materials[5,33].

Syngas production by RWGS-CL has several advantages over solar thermochemical processes. By using H_2 for material reduction, temperatures can be lowered significantly. Although in this analysis a reactor temperature of 1073 K was assumed, operating temperatures as low as 823 K have been reported for RWGS-CL[5]. Contrary to solar thermochemical processes, reduced pressure is not needed in RWGS-CL since oxidation and reduction are equimolar reactions with respect to the gaseous components. This potentially leads to lower equipment and operating costs. Furthermore, in isothermal operation solid phase heat recuperation can be omitted. Oxidation and reduction can be carried out at constant temperature. Since both reactions are endothermic, no heat is produced. Thus, there is no need for solid phase heat recuperation in the reactor. Furthermore, hot spots which often occur in exothermic reactions and may damage the oxygen storage material can be avoided. The use of H_2 for material reduction increases the difference in attainable oxidation states compared to solar thermochemical processes, which only use a small range in material non-stoichiometry (e.g. ceria-based)[29]. For iron oxide, the thermodynamically possible CO yield per cycle is $17.2\,\mathrm{mol_{CO}/kg_{Fe_3O_4}}$, which is nearly 30 times the amount that can be produced by using

cerium oxide. Assuming a cycle between CeO_2 and $CeO_{2-\delta}$ with a non-stoichiometry of $\delta = 0.1$, a maximum CO yield of $0.58\,mol_{CO}/kg_{CeO_2}$ is achievable per cycle. Daza *et al.* reported a CO yield of approximately $4\,mol_{CO}/kg$ of $La_{0.75}Sr_{0.25}CoO_{3-\delta}$ for the RWGS-CL process[4]. A higher CO yield per cycle can potentially reduce the reactor size and minimize the equipment cost.

Theoretical overall efficiencies exceeding 20% have been reported for solar thermochemical syngas production by several groups[8,13,31]. However, the system boundary in these studies often includes only the reactor and gas phase heating and cooling. The energy demand of important ancillary process steps (e.g. vacuum pumping, sweep gas production, gas separation) is often disregarded, leading to very optimistic process efficiencies. Studies that include these process steps deliver more realistic values for the efficiency. Bulfin *et al.* estimated the maximum efficiency of solar thermochemical production of syngas to be 7.5% without heat recovery and 11.5% for 60% solid phase heat recovery[9]. Bader *et al.* estimated realistic efficiencies to be 10% and 18% for solar thermochemical production of H_2 and CO, respectively[10]. For a reduction temperature of 1800 K, Falter *et al.* estimated a realistic efficiency of approximately 16%[34]. These results are still optimistic taking into account the practical problems associated with solar thermochemical processes discussed above, which makes large scale implementation a rather distant reality. In contrast, efficiencies of up to 14.2% and 14.4% could be achieved by using the RWGS or the RWGS-CL process, respectively, with state-of-the-art equipment.

Conclusions

Thermodynamic analysis was performed to compare RWGS and RWGS-CL based on idealized process systems. The energy demand for product separation was estimated based on literature data of separation processes. The difference in process efficiency between RWGS and RWGS-CL is most pronounced for syngas with a low H_2/CO ratio. The energy demand for H_2 production contributes most to the StS efficiency (η_{StS}). Without considering the energy demand of the electrolyzer, the energy consumption for the reactor/separator sequence can be reduced by up to 54% using the RWGS-CL process as compared to the conventional RWGS process. Heat integration reduces the energy demand for process stream heating by up to 70%, depending on the desired syngas H_2/CO ratio. For pure CO production with heat integration, StS efficiencies of 12.7% and 13.7% can be achieved for RWGS and RWGS-CL, respectively. The syngas H_2/CO ratio in RWGS is adjusted either by adjusting the H_2/CO_2 ratio in the reactor or by adding H_2 after the reaction. The preferred method

depends strongly on the desired syngas H_2/CO ratio and if gas phase heat is integrated. The proposed process schemes for RWGS and RWGS-CL offer reasonable alternatives for solar syngas production with efficiencies comparable to solar thermochemical processes. RWGS-CL is advantageous especially for the production of pure CO.

Nomenclature

	Abbreviations	
PEM	Polymer electrolyte membrane	
RWGS	Reverse water-gas shift	
RWGS-CL	Reverse water-gas shift chemical looping	
	Symbols	
η_S	Separation efficiency	$[-]$
η_{StE}	Solar-to-electric efficiency	$[-]$
η_{StS}	Solar-to-syngas efficiency	$[-]$
σ	Stefan-Boltzmann constant	$[\mathrm{W \cdot m^{-2} \cdot K^{-4}}]$
$\dot{\xi}$	Reaction extent	$[\mathrm{mol \cdot s^{-1}}]$
c_p	Molar heat capacity	$[\mathrm{J \cdot mol^{-1} \cdot K^{-1}}]$
C	Solar concentration factor	$[-]$
F	Dimensionless energy factor	$[-]$
G_0	Nominal solar flux incident	$[\mathrm{W \cdot m^{-2}}]$
h	Molar enthalpy	$[\mathrm{J \cdot mol^{-1}}]$
$\dot{H}$	Enthalpy flow	$[\mathrm{J \cdot s^{-1}}]$
HHV	Higher heating value	$[\mathrm{J \cdot mol^{-1}}]$
ΔH_R	Heat of reaction	$[\mathrm{J \cdot mol^{-1}}]$
K_{eq}	Reaction equilibrium constant	$[-]$
L_H	Heat loss factor	$[-]$
$\dot{N}$	Molar flow	$[\mathrm{mol \cdot s^{-1}}]$
p	Pressure	[Pa]
$\dot{Q}$	Heat flow	$[\mathrm{J \cdot s^{-1}}]$
R	Universal gas constant	$[\mathrm{J \cdot mol^{-1} \cdot K^{-1}}]$
T	Temperature	[K]
$\dot{W}$	Work flow/Power	$[\mathrm{J \cdot s^{-1}}]$
x	Mole fraction	$[-]$

List of Figures

References

[1] IPCC . Climate Change 2013: The Physical Science Basis. Working Group I Contribution to the Fifth Assessment Report of the Intergovernmental Panel on Climate Change. *Cambridge University Press.* 2014.

[2] Hiller H, Reimert R, Stönner H-M. Gas Production, 1. Introduction. in *Ullmann's Encyclopedia of Industrial Chemistry*:403–421Wiley-VCH Verlag GmbH & Co. KGaA 2000.

[3] Mallapragada DS, Singh NR, Curteanu V, Agrawal R. Sun-to-Fuel Assessment of Routes for Fixing CO_2 as Liquid Fuel. *Industrial & Engineering Chemistry Research.* 2013;52:5136–5144.

[4] Daza YA, Kent RA, Yung MM, Kuhn JN. Carbon Dioxide Conversion by Reverse Water-Gas Shift Chemical Looping on Perovskite-Type Oxides. *Industrial & Engineering Chemistry Research.* 2014;53:5828–5837.

[5] Daza YA, Maiti D, Kent RA, Bhethanabotla VR, Kuhn JN. Isothermal Reverse Water Gas

Shift Chemical Looping on $La_{0.75}Sr_{0.25}Co_{(1-Y)}Fe_YO_3$ Perovskite-type Oxides. *Catalysis Today.* 2015;258, Part 2:691–698.

[6] Daza YA, Kuhn JN. CO_2 conversion by reverse water gas shift catalysis: Comparison of catalysts, mechanisms and their consequences for CO_2 conversion to liquid fuels. *RSC Adv.* 2016;6:49675–49691.

[7] Romero M, Steinfeld A. Concentrating Solar Thermal Power and Thermochemical Fuels. *Energy Environ. Sci..* 2012;5:9234–9245.

[8] Scheffe JR, Steinfeld A. Thermodynamic Analysis of Cerium-Based Oxides for Solar Thermochemical Fuel Production. *Energy & Fuels.* 2012;26:1928–1936.

[9] Bulfin B, Call F, Lange M, et al. Thermodynamics of CeO_2 Thermochemical Fuel Production. *Energy & Fuels.* 2015;29:1001–1009.

[10] Bader R, Venstrom LJ, Davidson JH, Lipiński W. Thermodynamic Analysis of Isothermal Redox Cycling of Ceria for Solar Fuel Production. *Energy & Fuels.* 2013;27:5533–5544.

[11] Krenzke PT, Davidson JH. Thermodynamic Analysis of Syngas Production via the Solar Thermochemical Cerium Oxide Redox Cycle with Methane-Driven Reduction. *Energy & Fuels.* 2014;28:4088–4095.

[12] Loutzenhiser PG, Steinfeld A. Solar Syngas Production from CO_2 and H_2O in a Two-step Thermochemical Cycle via Zn/ZnO Redox Reactions: Thermodynamic Cycle Analysis. *International Journal of Hydrogen Energy.* 2011;36:12141–12147.

[13] Gálvez ME, Loutzenhiser PG, Hischier I, Steinfeld A. CO_2 Splitting via Two-Step Solar Thermochemical Cycles with Zn/ZnO and FeO/Fe_3O_4 Redox Reactions: Thermodynamic Analysis. *Energy & Fuels.* 2008;22:3544–3550.

[14] Marxer D, Furler P, Scheffe JR, et al. Demonstration of the Entire Production Chain to Renewable Kerosene via Solar Thermochemical Splitting of H_2O and CO_2. *Energy & Fuels.* 2015;29:3241–3250.

[15] Kim J, Henao CA, Johnson TA, et al. Methanol Production From CO_2 Using Solar-Thermal Energy: Process Development and Techno-economic Analysis. *Energy Environ. Sci..* 2011;4:3122–3132.

[16] Kim J, Johnson TA, Miller JE, Stechel EB, Maravelias CT. Fuel Production From CO_2 Using Solar-Thermal Energy: System Level Analysis. *Energy Environ. Sci..* 2012;5:8417–8429.

[17] Furler P, Scheffe JR, Steinfeld A. Syngas Production by Simultaneous Splitting of H_2O and CO_2 via Ceria Redox Reactions in a High-Temperature Solar Reactor. *Energy Environ. Sci..* 2012;5:6098–6103.

[18] Ermanoski I, Siegel NP, Stechel EB. A New Reactor Concept for Efficient Solar-Thermochemical Fuel Production. *Journal of Solar Energy Engineering-Transactions of the ASME.* 2013;135.

[19] Gueymard CA. The sun's total and spectral irradiance for solar energy applications and solar radiation models. *Solar Energy.* 2004;76:423–453.

[20] Mancini T, Heller P, Butler B, et al. Dish-Stirling Systems: An Overview of Development and Status. *Journal of Solar Energy Engineering Transactions of the ASME.* 2003;125:135–151.

[21] Ferrero D, Lanzini A, Santarelli M, Leone P. A Comparative Assessment on Hydrogen Production from Low- and High-temperature Electrolysis. *International Journal of Hydrogen Energy.* 2013;38:3523–3536.

[22] Carmo M, Fritz DL, Mergel J, Stolten D. A comprehensive review on PEM water electrolysis. *International Journal of Hydrogen Energy.* 2013;38:4901–4934.

[23] Zoulias E, Varkaraki E, Lymberopoulos N. A review on water electrolysis. *TCJST.* 2004;4:41-71.

[24] Wilcox J. *Carbon Capture.* New York: Springer, 2012.

[25] Demirel Y. *Nonequilibrium Thermodynamics (2nd edition).* Amsterdam: Elsevier Science, 2007.

[26] House KZ, Baclig AC, Ranjan M, Nierop EA, Wilcox J, Herzog HJ. Economic and Energetic Analysis of Capturing CO_2 from Ambient Air. *Proceedings of the National Academy of Sciences.* 2011;108:20428–20433.

[27] Jarrett C, Chueh W, Yuan C, Kawajiri Y, Sandhage KH, Henry A. Critical Limitations on the Efficiency of Two-step Thermochemical Cycles. *Solar Energy.* 2016;123:57–73.

[28] Kemp IC. *Pinch analysis and process integration: A user guide on process integration for the efficient use of energy.* Oxford: Butterworth-Heinemann 2007.

[29] Agrafiotis C, Roeb M, Sattler C. A review on solar thermal syngas production via redox pair-based water/carbon dioxide splitting thermochemical cycles. *Renewable & Sustainable Energy Reviews.* 2015;42:254–285.

[30] Scheffe JR, Steinfeld A. Oxygen exchange materials for solar thermochemical splitting of H_2O and CO_2: A review. *Materials Today.* 2014;17:341–348.

[31] Ermanoski I, Miller JE, Allendorf MD. Efficiency maximization in solar-thermochemical fuel production: Challenging the concept of isothermal water splitting. *Physical Chemistry Chemical Physics.* 2014;16:8418.

[32] Lapp J, Davidson JH, Lipiński W. Efficiency of two-step solar thermochemical non-stoichiometric redox cycles with heat recovery. *Energy.* 2012;37:591–600.

[33] Dey S, Naidu BS, Rao CNR. $Ln_{0.5}A_{0.5}MnO_3$ (Ln = Lanthanide, $A = Ca, Sr$) Perovskites Exhibiting Remarkable Performance in the Thermochemical Generation of CO and H_2 from CO_2 and H_2O. *Chemistry - A European Journal.* 2015;21:7077–7081.

[34] Falter CP, Sizmann A, Pitz-Paal R. Modular reactor model for the solar thermochemical production of syngas incorporating counter-flow solid heat exchange. *Solar Energy.* 2015;122:1296–1308.